Intelligent model selection with updating parameters during staged excavation using optimization method

Yin-Fu JIN[1], Zhen-Yu YIN[1*], Wan-Huan ZHOU[2,*] and Xianfeng LIU[3]

Affiliation:

1 Department of Civil and Environmental Engineering, The Hong Kong Polytechnic University, Hung Hom, Kowloon, Hong Kong, China

2 State Key Laboratory of Internet of Things for Smart City and Department of Civil and Environmental Engineering, University of Macau, Macau S.A.R., China

3 Key Laboratory of High-Speed Railway Engineering of Ministry of Education, School of Civil Engineering, Southwest Jiaotong University, Chengdu, China

* Corresponding author: Dr Zhen-Yu Yin, Tel. +852 34008470, Fax +852 23346389, E-mail: zhenyu.yin@polyu.edu.hk; zhenyu.yin@gmail.com

Abstract: Various constitutive models have been proposed and previous studies focused on identifying parameters of specified models. To develop the smart construction, this paper proposes a novel optimization-based intelligent model selection procedure in which parameter identification is also performed during staged excavation. To conduct the model selection, a database of seven constitutive models accounting for isotropic or anisotropic yield surface, isotropic or anisotropic elasticity, or small strain stiffness for clayey soils is established, with each model numbered and deemed as one additional parameter for optimization. A newly developed real-coded genetic algorithm is adopted to evaluate the performance of simulation against field measurement. As the process of optimization goes on, the soil model exhibiting good performance during simulation survives from the database and model parameters are also optimized. For each excavation stage, with the selected model and optimized parameters, wall deflection and ground surface settlement of the subsequent unexcavated stage are predicted. The proposed procedure is repeated until the entire excavation is finished. This proposed procedure is applied to a real staged excavation with field data, which demonstrates its effectiveness and efficiency in engineering practice with highlighting the importance of anisotropic elasticity and small strain stiffness in simulating excavation. All results

demonstrate that the current study has both academic and practical significance in providing an efficient and effective approach of adaptive optimization-based model selection with parameters updating in engineering applications.

Key words: Constitutive relation; parameter identification; excavation; optimization; clay; finite element method

1 Introduction

Braced excavation poses a complicated problem of soil–structure interaction that can cause lateral wall deflection and ground movement (including lateral movement and surface settlement) that may damage adjacent buildings and utilities [1-4]. Accurately predicting lateral wall deflection and ground movement is important during excavation, providing as it does suggestions for subsequent construction. When analyzing an excavation's risk of accident, numerical calculation serves as a powerful tool supporting this aim. In numerical analysis, accurate prediction relies on both the selection of an appropriate soil model and the accuracy of corresponding model parameters [5-9]. Indeed the soil model selection is crucial in solving real engineering issues. It can give an accurate stress strain relationship for the soil involved in the excavation, allowing reasonable predictions of lateral wall deflection and ground movement. To date, hundreds of soil constitutive models have been proposed [10]. Not surprisingly, different constitutive models give different results during numerical simulation, prompting different engineering decisions that affect an excavation's levels of safety, economy, and risk. Existing studies, however, have chiefly focused on producing more accurate soil models, giving short shrift to evaluate applicability and selecting the most appropriate existing model. This study will serve as a remedy.

In practice, selection of a constitutive model often depends on the user's preferences and experiences, both of which are subjective. As a result, lack of attention to the problem of model selection has become a primary source of risk for accident. At present, model selection usually relies on a Bayesian probabilistic approach [11-17]. However, the use of the Markov Chain Monte Carlo (MCMC) method or other similar methods for this purpose makes such an approach time-consuming

when involving the finite element analysis (FEA). Furthermore, the parameters of constitutive model cannot be obtained during such a model selection process. Accordingly, a procedure able to automatically select the most appropriate soil model while simultaneously obtaining corresponding model parameters would be of considerable use to engineers. Recently, some optimization methods have offered certain advantages for selecting a model and identifying model parameters (Jin et al.[18-20,10,21]; Yin et al.[22,23]). Thus, a procedure for model selection and parameter identification that employs the optimization method in excavation offers competitive advantages.

The monitoring is essential for the practice of excavation, which can be found in many codes of different counties or regions [1, 24-30]. Normally prior to the excavation, the general plan for excavation should be prepared, which includes the detailed plans like how to excavate, how to monitor and how to avoid accident, etc. For instance, for deep excavation in soft clay deposit, the layered excavation must be carried out with the delamination depth less than 2 meters; the horizontal displacement of wall and the settlement of ground surface must be measured in real-time through the layout sensors or other monitoring devices. Therefore, engineers can benefit from the data of field measurements with some analyses to help them make a reliable decision thereby improving the excavation's levels of safety, economy, and risk. In the past, the real-time field measurements were used for Bayesian-based updating (Hsiao et al.[24], Junag et al.[1], Qi and Zhou et al.[25]) and the optimization-based updating (Finno and Calvello [26], Zhao et al.[27], Huang et al.[28], Jin et al.[29] and Levasseur et al.[30]).

Different from them, this paper proposes a procedure for intelligent model selection and concomitant parameter identification during staged excavation. First, a database of seven soil models accounting for different clay behaviors is proposed, using the Modified Cam-Clay model as its basis. Then an optimization-based procedure is proposed whereby the optimal model is automatically selected in the model database on the basis of simulation performance versus field measurements during excavation with the model parameters optimized simultaneously. With the selected model and optimized parameters, wall deflection and ground surface settlement of the subsequent unexcavated stage are predicted. The proposed procedure is repeated until the entire excavation is finished. The procedure is finally applied to a real staged excavation and validated by predicting deformations of subsequent stages with reference to field data.

2 Database of soil models

2.1 Brief introduction of Modified Cam-Clay model

When simulating the behavior of clays, the Modified Cam-Clay model (MCC) proposed by Roscoe and Burland [31] is ubiquitous in excavation [28,27]. Accordingly, it was selected as a base on which to form a database of soil models. The main constitutive equations of MCC model are:

$$f = \frac{3}{2} s_{ij} s_{ij} + M^2 p' \left(p' - p_m \right) \tag{1}$$

$$\delta p_m = p_m \left(\frac{1 + e_0}{\lambda - \kappa} \delta \varepsilon_v^p \right) \tag{2}$$

$$\delta \varepsilon_{ij}^p = d\lambda \frac{\partial f}{\partial \sigma'_{ij}} \tag{3}$$

where f is the yield surface (see Fig. 1(a)), p' the mean effective stress, q the deviatoric stress, p_m the size of the yield surface, κ the swelling index; λ the compression index, e_0 the initial void ratio, $d\lambda$ the plastic multiplier, $\delta\varepsilon_{ij}^{p}$ the tensor of incremental plastic strain, σ'_{ij} the effective stress tensor, and M the critical state value of the stress ratio η (where $\eta = q/p'$).

To describe the Lode angle dependent shear strength, the M is expressed as follows according to Sheng et al. [32],

$$M = M_c \left[\frac{2c^4}{1 + c^4 + (1 - c^4)\sin 3\theta} \right]^{\frac{1}{4}} \tag{4}$$

where M_c is the slope of critical state line in compression, $c = (3 - \sin\phi_c)/(3 + \sin\phi_c)$, according to Mohr-Coulomb yield criterion (ϕ_c is the friction angle); the lode angle is expressed as $\frac{-\pi}{6} \le \theta = \frac{1}{3}\sin^{-1}\left(\frac{-3\sqrt{3}J_3}{2J_2^{3/2}}\right) \le \frac{\pi}{6}$ using $J_2 = \frac{1}{2}s_{ij} : s_{ij}$, $J_3 = \frac{1}{3}s_{ij}s_{jk}s_{ki}$ with $s_{ij} = \sigma_{ij} - p'\delta_{ij}$. This can also be replaced by the transformed stress method of (Yao et al. [33-35]).

2.2 Anisotropy of yield surface

Natural clays usually exhibit a significant degree of anisotropy of yield surface developed during geological deposition and a subsequent change of this anisotropy due to loading. Neglecting this anisotropy could produce inaccurate predictions of soil response during excavation [36,37]. Thus, the initial and induced anisotropy of yield surface should be a component of the clay behavior during simulating excavation. According to Wheeler et al. [38], such anisotropy can be incorporated into

MCC by introducing a state variable α to the yield function, thereby producing the model "S-CLAY1" (see Fig. 1(b)).

$$f = \frac{3}{2}\left(s_{ij} - p'\bar{\alpha}_{ij}\right)\left(s_{ij} - p'\bar{\alpha}_{ij}\right) + \left(M^2 - \frac{3}{2}\bar{\alpha}_{ij}\bar{\alpha}_{ij}\right)p'\left(p' - p_m\right) \tag{5}$$

$$\delta\bar{\alpha}_{ij} = \omega\left[\left(\frac{3s_{ij}}{4p'} - \bar{\alpha}_{ij}\right)\left\langle\delta\varepsilon_v^p\right\rangle + \omega_d\left(\frac{s_{ij}}{3p'} - \bar{\alpha}_{ij}\right)\delta\varepsilon_d^p\right] \tag{6}$$

in which $\alpha = \sqrt{2/3\left(\bar{\alpha}_{ij} : \bar{\alpha}_{ij}\right)}$ is defined with $\bar{\alpha}_{ij} = \begin{bmatrix}\alpha_x - 1 & \alpha_y - 1 & \alpha_z - 1 & \sqrt{2}\alpha_{xy} & \sqrt{2}\alpha_{yz} & \sqrt{2}\alpha_{zx}\end{bmatrix}$; the calculation of Lode angle is modified as $\frac{-\pi}{6} \le \theta = \frac{1}{3}\sin^{-1}\left(\frac{-3\sqrt{3}\bar{J}_3}{2\bar{J}_2^{3/2}}\right) \le \frac{\pi}{6}$ using $\bar{J}_2 = \frac{1}{2}\bar{s}_{ij} : \bar{s}_{ij}$, $\bar{J}_3 = \frac{1}{3}\bar{s}_{ij}\bar{s}_{jk}\bar{s}_{ki}$ with $\bar{s}_{ij} = s_{ij} - p'\bar{\alpha}_{ij}$.

In the anisotropy of yield surface, p_m and α define the size and inclination of the yield curve, respectively, whereas α is a measure of the degree of plastic anisotropy of the soil. With α=0, soil behavior is isotropic and Eq.(5) can be reduced to the MCC yield function. The initial preconsolidation pressure obtained from oedometer test, can be used as an input for calculating the initial size p_m from Eq.(5). ε_v^p and ε_d^p are volumetric and deviatoric plastic strains, respectively. The two parameters ω and ω_d controlling the rotational hardening of yield surface can be directly calculated as follows (Wheeler et al. [38]; Leoni et al. [39]; Yin et al. [40,41]):

$$\alpha_0 = \alpha_{K_0} = \eta_{K_0} - \frac{M_c^2 - \eta_{K0}^2}{3} \text{ with } \eta_{K_0} = \frac{3M_c}{6 - M_c} \tag{7}$$

$$\omega = \frac{1 + e_0}{\left(\lambda - \kappa\right)}\ln\frac{10M_c^2 - 2\alpha_{K_0}\omega_d}{M_c^2 - 2\alpha_{K_0}\omega_d} \text{ with } \omega_d = \frac{3\left(4M_c{}^2 - 4\eta_{K0}^2 - 3\eta_{K0}\right)}{8\left(\eta_{K0}^2 + 2\eta_{K0} - M_c{}^2\right)} \tag{8}$$

Thus, no input parameters are needed for the anisotropy of yield surface.

2.3 Inherent cross-anisotropy of elasticity

Apart from the anisotropic plasticity, the soil always exhibits naturally inherent cross-anisotropy of elasticity, which significantly effects lateral wall deflection and ground movement during excavation (Teng et al. [7]). Anisotropic elastic behavior, which is also important and can be taken into account by means of the following compliance matrix of elastic stiffness:

$$\begin{bmatrix} \delta\varepsilon_x \\ \delta\varepsilon_y \\ \delta\varepsilon_z \\ \delta\varepsilon_{xy} \\ \delta\varepsilon_{yz} \\ \delta\varepsilon_{zx} \end{bmatrix} = \begin{bmatrix} 1/E_v & -\upsilon'_{vv}/E_v & -\upsilon'_{vv}/E_v & 0 & 0 & 0 \\ -\upsilon'_{vv}/E_v & 1/E_h & -\upsilon'_{vh}/E_h & 0 & 0 & 0 \\ -\upsilon'_{vv}/E_v & -\upsilon'_{vh}/E_h & 1/E_h & 0 & 0 & 0 \\ 0 & 0 & 0 & 1/2G_{vh} & 0 & 0 \\ 0 & 0 & 0 & 0 & \left(1+\upsilon'_{vh}\right)/E_h & 0 \\ 0 & 0 & 0 & 0 & 0 & 1/2G_{vh} \end{bmatrix} \begin{bmatrix} \delta\sigma'_x \\ \delta\sigma'_y \\ \delta\sigma'_z \\ \delta\sigma'_{xy} \\ \delta\sigma'_{yz} \\ \delta\sigma'_{zx} \end{bmatrix} \tag{9}$$

with $E_h = nE_v$, $\upsilon'_{vh} = \sqrt{n}\upsilon'_{vv}$, where E_v and E_h are the vertical and horizontal Young's modulus, respectively, υ'_{vv} and υ'_{vh} are the vertical and horizontal Poisson's ratio, respectively, and G_{vh} is the shear modulus (see Graham and Houlsby [42]). Alternatively, different definitions for the vertical and horizontal Poisson's ratio can also be found as υ'_{vh} and υ'_{hh} in works of Hoque and Tatsuoka [43] and Hicher and Chang[44]. For stress-controlled isotropic compression with incremental stress of $\delta\sigma'_x = \delta\sigma'_y = \delta\sigma'_z = \delta p'$,

$$\delta\varepsilon_v = \delta\varepsilon_x + \delta\varepsilon_y + \delta\varepsilon_z = \left(1 - 4\upsilon'_{vv} + 2/n - 2\upsilon'_{vv}/\sqrt{n}\right)\frac{\delta p'}{E_v} \tag{10}$$

Based on the definition of bulk modulus, $K=\delta p'/\delta\varepsilon_v$, the vertical Young's modulus can be obtained as follows, with the shear modulus, G_{vh}:

$$E_v = \left(1 - 4\upsilon'_{vv} + 2/n - 2\upsilon'_{vv}/\sqrt{n}\right)\left(\frac{1+e_0}{\kappa}\right)p' \tag{11}$$

$$G_{vh} = \frac{\sqrt{n}E_v}{2\left(1+\sqrt{n}\upsilon'_{vv}\right)} \tag{12}$$

Then, only one additional parameter n is needed to introduce the anisotropic elasticity.

2.4 Small strain stiffness

As already noted, small strain stiffness behavior significantly influences predictions of excavation-induced settlement. It is generally recognized that ground settlement is more difficult to be accurately predicted than lateral wall deflection, even when relying on well-measured soil parameters derived from laboratory test or field observation. Many studies have demonstrated, however, that ground settlement can be accurately predicted by means of an appropriate soil model that considers soil's small strain stiffness behavior [6,5,45]. The degradation of stiffness with increasing strain has been expressed by various relationships (Benz [46]), but all such expressions ignore the effect of volumetric strain on stiffness degradation. In fact, isotropic and K_0 compression tests with unloading-reloading loops on different clays indicated the increasing of κ (corresponding to the degradation of Bulk modulus) due to the volumetric strain (shown in Fig. 2, Reconstituted Bothkennar clay by Allman and Atkinson [47], and Kaolin clay by Hattab and Hicher [48]). Considering a constant Poisson's ratio, the effect of volumetric strain to the shear modulus should also be considered.

According to Hardin and Drnevich [49], the shear modulus G was expressed as:

$$G = \frac{G_0}{1+\left|\frac{\gamma}{\gamma_a}\right|} \tag{13}$$

Using the threshold shear strain $\gamma_a=\gamma_{0.7}$, Santos and Correia [43] have put forward the following modified Hardin-Drnevich relationship:

$$G = \frac{G_0}{1+a\left(\frac{\gamma}{\gamma_{0.7}}\right)} \tag{14}$$

where the constant a=3/7 is obtained by Santos and Correia [43] through curve fitting from many test results. According to Benz [39], the secant modules given in Eq.(14) should be converted to a tangent modulus for the convenience in numerical application:

$$G = \frac{G_0}{\left(1+a\frac{\gamma}{\gamma_{0.7}}\right)^2} \tag{15}$$

Taking the $\gamma_{ref}=\gamma_{0.7}/a$, the Eq.(15) can be simplified as,

$$G = \frac{G_0}{\left(1+\gamma/\gamma_{ref}\right)^2} \tag{16}$$

where the shear strain γ can be replaced by the deviatoric strain ε_d for the extension, and $\gamma_{ref}=7\varepsilon_{70}/3$ is defined with ε_{70} the deviatoric strain level corresponding to 70% of maximum stiffness. For simplicity's sake, adopting the shear modulus at 0.1 % of strain $G_{0.1\%}$ as the input parameter, the initial shear modulus G_0 can be obtained:

$$G_0 = \left(1+0.001/\gamma_{ref}\right)^2 G_{0.1\%} \tag{17}$$

For clayey soils, $G_{0.1\%}$ can be calculated using swelling index κ as:

$$G_{0.1\%} = \frac{(1-2\upsilon)}{2(1+\upsilon)} \frac{(1+e_0)}{\kappa} p' \tag{18}$$

Thus, the shear modulus G can be expressed as:

$$G = \frac{\left(1+0.001/\gamma_{ref}\right)^2}{\left(1+\varepsilon_d/\gamma_{ref}\right)^2} \frac{(1-2\upsilon)}{2(1+\upsilon)} \frac{(1+e_0)}{\kappa} p' \tag{19}$$

To take into account the effect of volumetric strain for describing this stiffness degradation, a new relationship was proposed by modifying the swelling index κ (detailed in Appendix A):

$$\kappa_s = \frac{3(1-2\upsilon)(1+e_0)}{2(1+\upsilon)} \left(1 + P_{\text{rev}} \frac{3}{7} \left| \frac{\varepsilon_{eq}^*}{\varepsilon_{70}} \right| \right)^2 \frac{p_{at}}{G_{ref\,0}} \tag{20}$$

with,

$$G_{ref\,0} = \frac{3(1-2\upsilon)(1+e_0)}{2(1+\upsilon)} \left(1 + P_{\text{rev}} \frac{3}{7} \left| \frac{0.001}{\varepsilon_{70}} \right| \right)^2 \frac{p_{at}}{\kappa} \tag{21}$$

where κ_s is the apparent swelling index under strain level from small to large, P_{rev} is the controlling factor of stiffness with P_{rev} =1 when loading and P_{rev} =2 when unloading; $\varepsilon_{eq}^* = \sqrt{(\varepsilon_v)^2 + (\varepsilon_d)^2}$ is the average equivalent strain, ε_{70} is thus the equivalent strain level corresponding to 70% of maximum stiffness, p_{at} is atmospheric pressure p_{at}=101.325 kPa, and G_{ref0} is the initial reference secant stiffness. After obtaining the apparent swelling index κ_s, the elastic modulus E_v in Eq. (11) can be calculated by replacing κ with κ_s. So using above equations, the κ is still used as input parameter and only one additional parameter ε_{70} is required. Fig. 3 shows the evolutions of stiffness degradation for

different values of ε_{70}. The value of ε_{70} can be related to plasticity index (PI) for clayey soils according to database of Benz [46], as shown in Fig. 4.

Note that the proposed small-strain stiffness relationship for capturing stress-strain hysteresis loop, which is also an important feature of soils during cyclic loading, ~~cyclic loading behavior~~ can be achieved by the stress reversal technique proposed by Yin et al. [50] with the definition of ε_{eq}^{*} as follows,

$$\varepsilon_{eq}^{*}=\sqrt{\frac{2}{3}\left(e_{ij}-e_{ij}^{R}\right):\left(e_{ij}-e_{ij}^{R}\right)+\left(\varepsilon_{v}-\varepsilon_{v}^{R}\right)^{2}} \tag{22}$$

where e_{ij}^{R} is the deviatoric strain tensor at reverse point and ε_{v}^{R} is the volumetric strain at reverse point. Then, the model can be applied to more general cases with complicated loading conditions. In order to make sure of activating the strain at reversal points and the elastic anisotropy controlling by the parameters of ε_{70} and n, three simulations of an undrained triaxial test with loading-unloading-reloading phases were conducted with values of other parameters taken from the 2nd layer of soils (depth from 8 m to 33 m) in Table 3. As shown in Fig. 5, the stress-strain hysteresis loop has been well described by the implementation of small strain stiffness ($\varepsilon_{70} = 10^{-4}$ compared to $\varepsilon_{70} = 0$), and the elastic anisotropy has been well described by the incorporation of a transversely isotropic elasticity ($n = 1.5$ compared to $n = 1$). Note that in this study, the soils of interest during excavation are under a condition without involving cyclic loading. The stress reversal technique and bounding or subloading surface concept are ~~is~~ not needed under such a condition.

Overall, based on MCC model, a database of seven soil models with different features can be obtained, as summarized in Table 1. All models were implemented into a commercial finite element code ABAQUS via UMAT [21,22]. The parameters of all soil models can be divided into four groups: (1) MCC related parameters, υ, e_0, κ, λ, M_c, and σ'_{p0}; (2) anisotropic plasticity related parameters, α_0, ω, and ω_d using Eqs.(7) and (8); (3) anisotropic elasticity related parameter, n; and (4) small strain stiffness related parameter, ε_{70}. Note that for the isotropic yield surface "$\alpha_0 = \omega = \omega_d = 0$" is assigned, and for no consideration of small strain stiffness ε_{70}=0 is given.

3 Model selection strategy in a staged excavation

This section presents a procedure for selecting a model as the excavation proceeds, based on optimization during which wall deflection and ground surface settlement predictions for the next unexcavated stage were simultaneously obtained. This procedure thus seeks to simultaneously find the most appropriate soil model and its optimal parameters.

For simplicity's sake, and to aid model selection, each model in the database was marked with a sequence number corresponding to the soil model in the optimization. The sequence numbers associated with the model parameters composed a set of variables in the optimization. Such variables were simultaneously identified using the optimization algorithm, based on the observed excavation field data.

The pseudocode for identifying a model by sequence number is presented herein, with the variable *model_selection* first defined as an integer of value ranging from 1 to 7. Next, seven

different cases corresponding to seven different soil models, were built. The soil model used in the FEA will be automatically chosen according to the value of *model_selection*.

The pseudocode of the model selection is given below:

switch *model_selection*
    case 1 % MCC
        $\alpha_0 = \omega = \omega_d = 0$; $n=1$; $\varepsilon_{70}=0$
    case 2 % S-CLAY1
        α_0, ω, and $\omega_d \neq 0$ (using Eqs.(7) and (8)); $n=1$; $\varepsilon_{70}=0$
    case 3 % MCC-AE
        $\alpha_0 = \omega = \omega_d = 0$; $n\neq 1$; $\varepsilon_{70}=0$
    case 4 % MCC-SS
        $\alpha_0 = \omega = \omega_d = 0$; $n=1$; $0<\varepsilon_{70}<10^{-3}$
    case 5 % S-CLAY1-AE
        α_0, ω, and $\omega_d \neq 0$ (using Eqs.(7) and (8)); $n\neq 1$; $\varepsilon_{70}=0$
    case 6 % S-CLAY1-SS
        α_0, ω, and $\omega_d \neq 0$ (using Eqs.(7) and (8)); $n=1$; $0<\varepsilon_{70}<10^{-3}$
    case 7 % S-CLAY1-AE-SS
        α_0, ω, and $\omega_d \neq 0$ (using Eqs.(7) and (8)); $n\neq 1$; $0<\varepsilon_{70}<10^{-3}$
end

During the model selection process, parameter identification was also conducted. Because MCC parameters can be easily and accurately measured from laboratory tests, κ, λ, and σ'_{p0} can be measured from an oedometer test and M_c from three triaxial tests at different confining pressures. Both test types are conventional and are widely used to determine parameters. Accordingly, the MCC parameters were not included in the proposed procedure. Furthermore, whether the anisotropic plasticity is chosen depends on the value of *model_selection*. Once the anisotropic plasticity is chosen, related parameters α_0, ω, and ω_d will be automatically calculated according to Eqs. (7) and (8). Thus, three anisotropic plasticity-related parameters were also not included in the proposed optimization procedure.

As a result, the parameters υ, n, and ε_{70} must eventually be optimized based on the observed field data during the model selection process, as summarized in Table 1 for different models. Fig. 6 presents a schematic plot of model selection associations with parameter identification. For example, two individuals (0.2, 0.6, $10^{-3.5}$, 2) and (0.3, 1.5, $10^{-4.5}$, 5) corresponding to the variables υ, n, ε_{70}, and *model_selection* are selected. For the individual (0.2, 0.6, $10^{-3.5}$, 2), *model_selection*=2 implies that "α_0, ω, $\omega_d \neq 0$", n=1, and ε_{70}=0 are actually adopted in the FEA, whereas n=0.6 and $\varepsilon_{70}=10^{-3.5}$ are not used. For individual (0.3, 1.5, $10^{-4.5}$, 5), "α_0, ω, $\omega_d \neq 0$", n=1.5, and ε_{70}=0 are used in the simulation. After performing the optimization operator (e.g., crossover, mutation), the new possible population (0.3, 1.2, 10^{-4}, 3) was generated according to the principles of employed operators. This means that the anisotropic elasticity temporarily exerts a relatively important influence on the deformation of excavation. As the process goes on, the soil model exhibiting good performance during simulation survives to the next generation. Ultimately, a model having essential features will be selected from the database and the corresponding parameters will be optimized.

During a staged excavation, the proposed procedure will be repeated at every excavation stage until the entire excavation is finished. For each given excavation stage, with the selected model and optimized parameters, wall deflection and ground surface settlement of the subsequent unexcavated stage will be predicted. Such predictions can help the engineer assess the serviceability and reliability of adjacent buildings and utilities in advance.

4 Optimization-based intelligent procedure

The intelligent procedure through optimization consists of: (1) the formulation of an error function measuring the difference between numerical and observational results, and (2) the selection of an optimization strategy that makes possible the search for the optimal solutions.

4.1 Error function

To carry out an inverse analysis, a function that can evaluate the error between observed and numerical results must be defined, and then minimized. For each observation involved in the optimization, the difference between the observation and the numerical prediction is measured by a norm value, referred to as an individual norm which forms an error function Error(x):

$$\text{Error}(x) \rightarrow \min \tag{23}$$

where x is a vector containing the variables to be optimized. Bound constraints are introduced on these variables,

$$x_l \leq x \leq x_u \tag{24}$$

where x_l and x_u are, respectively, the lower and upper bounds of x.

As the first step in the formulation of an error function, an expression for the individual norm must be established. In general, the individual norm is based on Euclidean measures between discrete points, comprising experimental and numerical results. To make the error independent of test type and number of measurement points, an advanced error function can be adopted (Levasseur et al.

[30]). The average difference between measured and simulated results is expressed using the least square method:

$$\text{Error}(\mathbf{X}) = \sqrt{\frac{1}{N}\sum_{i=1}^{N}\left(\frac{U_i^{obs} - U_i^{num}}{U_i^{obs}}\right)^2} \times 100 \tag{25}$$

where $\mathbf{X}$ is an *n*-sized vector of unknown model input parameters, N the number of observation points, U_i^{obs} the value corresponding to the *i*th point of observed data, and U_i^{num} the value corresponding to the *i*th point of simulated data.

The next step is the formulation of a final norm, a total error function, based on the individual norms computed using Eq.(25). Generally, for a braced excavation, lateral wall deflection and ground movement are two extremely important indicators of the influence of soil structure interaction on the excavation. To allow model selection and parameter identification, the objective error function should involve these two important indicators. When multiple types of measurements are to be simultaneously considered in the back-analysis of excavation, the generalized objective function can be expressed as a mono-objective optimization form,

$$\min\left[\mathbf{Error}(\mathbf{X})\right] = \min\left[\frac{\text{Error}_{\text{wall deflection}}(\mathbf{X}) + \text{Error}_{\text{ground movement}}(\mathbf{X})}{2}\right] \tag{26}$$

where $\text{Error}_{\text{wall deflection}}(\mathbf{X})$ is objective error calculated on lateral wall deflation in each excavation stage, and $\text{Error}_{\text{ground movement}}(\mathbf{X})$ is objective error calculated on ground movement in each excavation stage.

In this study, the importance of wall deflection and ground settlement is considered to be equal-that is each weighted at 0.5. For a general mono-objective problem, the solution having the least amount of objective error is usually selected as the optimal one, but considering the uncertainties of measurements as well as the heterogeneities of soils, the individual, whose error is smaller than a reference value defined by the user can be deemed satisfactory for this problem. Thus, more than one optimized satisfactory set of parameters can be selected with which to predict the wall deflection and ground settlement of subsequent unexcavated stages.

4.2 Model selection with parameter identification

Fig. 7 shows the identification procedure based on the successive use of two different components: the FEM model for simulating excavation and the optimization process for finding the optimal solution. For the optimization program, any powerful optimization algorithm can be employed to find the best solution [10,21-23]. For the numerical simulation process, the user can adopt various FEM analysis tools allowing the conduct of the excavation according to the requirements, for example, PLAXIS [51,26], or ABAQUS [28,27] or other such tools. This study used ABAQUS in which all models were implemented. Note that each model was numbered and deemed as one additional parameter in optimization.

Initialization of individuals is a key step for any optimization problem generating as it does the initial sets of parameters. This initial population is governed by the number of individuals, their domain (range), and the method for controlling the distribution of those individuals within that domain. Using a well-distributed sampling to generate the initial population can increase the

robustness of the algorithm while avoiding premature convergence. In accordance with the approach taken by Poles et al. [52], the SOBOL sampling method, proposed by Sobol [53], was adopted in the optimization algorithm to generate the initial population. This deterministic algorithm imitates the behavior of a random sequence, allowing uniform sampling in the design space.

4.3 Adopted real-coded genetic algorithm

The widely used genetic algorithm is a good choice for enhancing model selection. The genetic algorithm (GA) originally developed by Holland [54] simulates Darwinian natural selection and serves as a genetics computational model of the biological evolutionary process. It also allows searching for the optimal solution by simulating natural evolution. A novel real-coded genetic algorithm (RCGA) developed by Jin et al. [21] was adopted herein for model selection. This adopted RCGA incorporates a hybrid strategy with two outstanding crossovers to enhance the search ability, a dynamic random mutation to enlarge the diversity of the population and a local search to speed convergence. Various experimental results indicate that the adopted RCGA can readily solve back-analysis geotechnical engineering problems (Jin et al. [21]).

In this study, RCGA settings follow those of Jin et al. [21]. The initial population size was taken to be 10 times the number of decision variables for a uniform testing environment. The maximum number of generations was set to 60 giving reasonable consideration to calculation costs and the accuracy of results.

5 Application of intelligent procedure

To evaluate the effectiveness of the proposed model selection procedure, a well-known excavation site, that of Taipei National Enterprise Center (TNEC), was selected and solved by the proposed model selection procedure. The TNEC is a well-documented excavation site for which field monitoring and soil testing data have been recorded accurately and completely [2,55,7]. Accordingly, the TNEC excavation was used to illustrate the mono-objective optimization framework for model selection and parameter identification using the observed wall and/or ground responses in the staged excavation.

5.1 Numerical simulation of the TNEC excavation

For TNEC, the excavation width is 41.2 m, and the length of the 0.9 m thick diaphragm wall is 35 m. Excavation was performed using the top-down construction method in seven stages to a final excavation depth of 19.7m, during which the diaphragm wall was supported by 150 mm thick concrete floor slabs. Fig. 8 shows the soil profile and excavation depth for each stage. The ground consists of six alternating silty sand (SM) and silty clay (CL) layers overlying a thick gravel formation. The CL layers are mainly of low plasticity and slightly overconsolidated soft to medium clay. The gravel layer is located 46 m below the ground surface. More information about the TNEC excavation can be found in Ou et al. [2,55].

Fig. 9 shows the geometry and the finite element mesh of the TNEC excavation. In the simulation, because of the geometric symmetry, only half of the excavation was modeled under a plane strain condition. The overall model was 100 m long and 45 m high large enough to avoid

boundary constraints [28,27]. The excavation was conducted in seven stages, per Ou et al. [2,55]. The retaining structure, including the retaining wall and the struts, was assumed to be linear elastic, and the element type of the soil was a four-node bilinear rectangular. A spring element and a two-node linear beam element were adopted for the strut and the retaining wall, respectively. According to Ou et al. [2,55], the Poisson's ratio of the diaphragm wall was assumed to be 0.2 and the Young's modulus of the diaphragm wall used in the analysis was 12 GPa. The average nominal axial stiffness per unit width for the first strut level and the second strut level were 1,4980 and 6,4363 kN/m/m, respectively. As preloading forces were applied to the struts during the installation procedure, the strut forces were taken as 98.1 and 392 kN/m for the first and second temporal horizontal struts, respectively. The axial stiffness of the concrete floor slabs is assumed to be 14,6512 kN/m/m. The friction coefficient of the wall-soil interface is assumed to be a constant value of 0.273 due to the slight effect on wall deflection [27,28]. In this study, a drained condition was assumed and the effective stress constitutive models were used for both sand and clay, a reasonable approach consistent with previous studies [28,55,27].

Because the excavation zone was mostly filled with clays, model selection and parameter identification were conducted chiefly on three clay layers in the excavation. Accordingly, three sand layers were modeled by Mohr Coulomb (MC) model using the parameters summarized in Table 2, per previous studies [6,27]. Three clay layers were modeled using the soil models presented in Table 1. So as to focus on model selection and to reduce the cost of parameter identification, common parameters for seven soil models were not considered in the optimization but instead were obtained from previous studies [6,56,7].

Table 3 summarized the upper and lower bounds for υ, n, and ε_{70} and the parameters of MCC for three clay layers.

5.2 Results and discussion

Generally, the deformation of the diaphragm wall during deep excavation exhibits a cantilever shape and then changes into a concave shape at latter stages (e.g., after the first or second stage). According to Juang et al.[1], back-analysis for updating soil parameters and model selection based on field observations during the early stages of excavation might not be meaningful because of inevitable changes to the deformation pattern. Furthermore, back-analysis is not notably effective during early stages, because the excavation responses (maximum wall deflection and ground settlement) during these early stages are generally minor and are often prone to measurement errors. Furthermore, because the measured vertical settlement for stage 1 was not available, the parameter identification and model selection procedure began with stage 2.

Using the proposed procedure, model selection and parameter identification were conducted up to stage 7, stage by stage. During each optimization, the minimum objective error and the corresponding model, represented by the number defined beforehand for each generation, were recorded. Fig. 10 shows the evolutions of the minimum objective error and the corresponding model with increases in the generation number for stages 2–7. It can be seen that model 5 “S-CLAY1-AE” was selected as best for stages 2–3, and that model 7 “S-CLAY1-AE-SS” was finally selected as the best for stages 4–7. These results reveal that anisotropic elasticity and plasticity behaviors are important for simulating deep excavation in all excavated stages, as highlighted by previous studies

[7,37]. When simulating excavation, the consideration of the anisotropy of soils can help improve accuracy when predicting lateral soil movement beyond the diaphragm wall. However, the importance of small strain stiffness in accurately predicting excavation is increasingly significant with excavation depth. For model selection in stages 2–3, the optimal results might not reflect the importance of small strain stiffness for predicting wall deflection and ground settlement as a result of inevitable changes in deformation pattern and of small values of observation [1]. As excavation proceeds, the importance of small strain stiffness characteristics on capturing of ground settlement increases. The results demonstrate that the small strain stiffness of soils can help improve accuracy during simulations of vertical soil movement behind the diaphragm wall, consistent with the findings of previous studies [5,6,45].

To demonstrate the process of model selection, Fig. 11 shows the proportion of each model in all generations at stages 2–7. At the initial optimization stage (e.g., generation number less than 15), the best model cannot be determined. But as optimization proceeds, the model selection process becomes clear, allowing selection from the database of soil models by the adopted RCGA of a model featuring good simulation performance. In early generations, the RCGA explores the search space in search of new solutions, using the hybrid crossover strategy in the attempt. Then, to avoid trapping in a local optimum and to prevent diversity loss, the RCGA uses exploration in later generations. As generations progress, the RCGA algorithm tunes the trade-off between the optimal solution and diversity of population until it finds a global solution. Thus, the model selection is a dynamic process of adjustment during which model features significantly influence the outcome.

The parameters for the corresponding model were also identified by association with the model selection process. Fig. 12 shows the optimal parameters for stages 2–7 of TNEC excavation during the model selection process. The *x*-axis of the graph, from 1 to 7, denotes the seven stages of the excavation. Note that the optimal parameters changing with preceding the excavation stage by stage are reasonable due to the spatial variability of natural deposits [1,57,25,58,59]. For Poisson's ratio, a reasonable narrow range around the value of 0.3 was obtained. The cross-anisotropic elasticity ratio *n* for the soil layer 0–5.6 m is around 2.0 during early stages of excavation, but as the excavation proceeds, the weight of observations for the soil layers at 0–5.6 m in the optimization decreases, producing an unreasonable value of *n*. Another reason is the minor values of wall deflection and ground settlement, and the inevitable changes to the deformation pattern during these early stages. For the layer 8.0–33 m, the cross-anisotropic elasticity ratio *n* increases from 1.0 to 2.5 with subsequent excavation stages, consistent with the test results obtained by Teng et al. [7]. Because small strain stiffness was not considered when selecting a soil model for stages 2 and 3, variations in small strain stiffness are shown for stages 4–7. For the soil layer 0–5.6 m, ε_{70} varies from 5×10^{-4} to 10^{-3}, less than seen in the empirical equation using the Atteberg limits $\varepsilon_{70}=5\times10^{-5}\exp(0.0639I_p)$, reported by Vucetic and Dobry [60] and Yin et al. [61]. For the soil layer 8.0–33 m, ε_{70} varies from 7×10^{-4} to 7×10^{-5}, which is reasonable. All optimal parameters demonstrate the effectiveness of the proposed parameter identification procedure combined with the advanced constitutive model.

Thus, accurate prediction of wall deflection and ground settlement can be achieved when obtained parameters as well as the selected model are reasonable and accurate. The accuracy of settlement predictions is an indicator of serviceability and reliability for adjacent buildings and

utilities, which is important for protecting their integrity. To evaluate the accuracy of identified parameters, wall deflection and ground settlement for the next unexcavated stage were predicted using the selected model with the corresponding optimal parameters, with the difference between predictions and observations evaluated, to reveal the effectiveness of the proposed procedure. Fig. 13 compares observations and predictions for wall deflection with error bars, and Fig. 14 compares the observations and predictions for ground settlement with error bars. In the former case, deformation pattern and maximum wall deflection are well predicted by the selected model using optimal parameters, making the performance of predictions of precision and accuracy for wall deflection acceptable in practice. In the latter case, predictions for stages 5–7 are acceptable for both maximum ground settlement and the influence zone induced by the excavation. All these results indicate the efficiency of the proposed optimization procedure for model selection and parameter identification.

Updating of wall deflection and ground settlement predictions followed by model selection and parameter identification resembles the Bayesian updating conducted by Juang et al. [1], with the difference that the proposed optimization-based procedure can accurately predict deformation of both magnitude and position, whereas Bayesian updating can only predict maximum deformation. Furthermore, when using a numerical model as the calculation tool for Bayesian updating, calculation time is prolonged as a result of more than 10,000 calculations that the Markov chain Monte Carlo (MCMC) sampling method requires to derive the posterior distributions of soil parameters—making it impractical for use. Accordingly, the proposed optimization-based procedure for model selection and parameter identification deserves to be applied in actual practice.

6 Conclusions

Selection of an appropriate model for solving the excavation problem is vital, thus to make accurate predictions and thereby reduce risk. In this paper, then, an optimization-based procedure for model selection and parameter identification has been proposed.

To conduct the model selection, a database of seven soil models was formed on the basis of the MCC model. In hopes of reproducing the behavior of natural clays, anisotropic plasticity, anisotropic elasticity, and small strain stiffness were adopted as the common features from which to form six models based on the MCC model. In the course of optimization, each soil model was considered as a possible choice in conjunction with the numerical model to simulate the excavation.

Then a novel model selection procedure was proposed based on optimization for excavation, according to which each soil model was represented by a variable: an integer varying from 1 to 7. The variable, together with the model parameters, was put into the optimization, in which the soil model used in the numerical model was determined by the value of the variable. The model parameters for optimization were chosen to suit the selected soil model, and the most appropriate soil model—with optimal parameters—was identified with an eye to minimize the error between simulation and observation (e.g., wall deflection and ground surface settlement). Using the selected model with optimal parameters, the wall deflection and ground settlement of the next unexcavated stage were predicted. For excavation, model selection with parameter identification and updating of wall deflection and ground settlement predictions were conducted stage by stage.

To finish, the effectiveness and efficiency of the proposed model selection procedure were evaluated by conducting a case study of the TNEC excavation with its seven stages. The wall deflection and ground surface settlement observed were used as the optimization objectives, with a mono-objective framework having two sub-objectives adopted for the TNEC excavation. Model selection was conducted starting from stage 3 lest inevitable early-stage changes to deformation pattern. The S-CLAY1-AE-SS model was identified as best by the adopted RCGA after stage 3, and the S-CLAY1-AE model until then. The selected model demonstrated the importance of anisotropic plasticity, cross-isotropic elasticity, and small strain stiffness behaviors in the simulation of an excavation.

The accuracy of predictions regarding the next unexcavated zones was verified by comparison to the observations measured after excavation, indicating high levels of effectiveness and efficiency for the proposed model selection procedure. All results demonstrated that the proposed optimization-based procedure for intelligent model selection and parameter identification deserves to be applied in actual practice.

Acknowledgments

This research was financially supported by the Research Grants Council (RGC) of Hong Kong Special Administrative Region Government (HKSARG) of China (Grant No.: PolyU R5037-18F, 15209119); Joint research project between SiChuan Province and National Universities funded by Science & Technology Department of Sichuan Province (No.2019YFSY0015), and Open research grant of MOE Key Laboratory of High-speed Railway Engineering.

Appendix A: Derivation of initial reference shear modulus and apparent swelling index

Based on Eq. (17), the shear modulus at 0.1 % of strain and that at any strain level is defined as

$$\begin{cases} G_{0.1\%} = \dfrac{G_0}{\left(1+0.001/\gamma_{ref}\right)^2} \\ G = \dfrac{G_0}{\left(1+\gamma/\gamma_{ref}\right)^2} \end{cases} \tag{A1}$$

According to the elasticity, the corresponding bulk modulus at 0.1 % of strain and that at any strain level is obtained

$$\begin{cases} K_{0.1\%} = \dfrac{2(1+\upsilon)}{3(1-2\upsilon)} G_{0.1\%} = \dfrac{2(1+\upsilon)}{3(1-2\upsilon)} \dfrac{G_0}{\left(1+0.001/\gamma_{ref}\right)^2} \\ K = \dfrac{2(1+\upsilon)}{3(1-2\upsilon)} G = \dfrac{2(1+\upsilon)}{3(1-2\upsilon)} \dfrac{G_0}{\left(1+\gamma/\gamma_{ref}\right)^2} \end{cases} \tag{A2}$$

Assuming the ordinary swelling index κ is adopted to computer the $K_{0.1\%}$ and a modified swelling index κ_s corresponding to any strain level is adopted to computer K

$$\begin{cases} K_{0.1\%} = \dfrac{(1+e_0)}{\kappa} p' \\ K = \dfrac{(1+e_0)}{\kappa_s} p' \end{cases} \tag{A3}$$

Combining the Eqs.(A2) and (A3), and noting a reference value p_{at} for replacing p', the initial reference shear modulus G_{ref0} for replacing G_0 can be defined as

$$\begin{cases} G_{ref\,0} = \dfrac{3(1-2\upsilon)(1+e_0)}{2(1+\upsilon)} \left(1+0.001/\gamma_{ref}\right)^2 \dfrac{p_{at}}{\kappa} \\ G_{ref\,0} = \dfrac{3(1-2\upsilon)(1+e_0)}{2(1+\upsilon)} \left(1+\gamma/\gamma_{ref}\right)^2 \dfrac{p_{at}}{\kappa_s} \end{cases} \tag{A4}$$

Adopting the $\gamma_{ref} = 7\varepsilon_{70}/3$, and adding a controlling factor of stiffness P_{rev} (with P_{rev} =1 when loading and P_{rev} =2 when unloading), the Eq.(A4) can be expressed as

$$\begin{cases} G_{ref\,0} = \dfrac{3(1-2\upsilon)(1+e_0)}{2(1+\upsilon)} \left(1+P_{\text{rev}} \dfrac{3}{7}\left|\dfrac{0.001}{\varepsilon_{70}}\right|\right)^2 \dfrac{p_{at}}{\kappa} \\ G_{ref\,0} = \dfrac{3(1-2\upsilon)(1+e_0)}{2(1+\upsilon)} \left(1+P_{\text{rev}} \dfrac{3}{7}\left|\dfrac{\varepsilon^*_{eq}}{\varepsilon_{70}}\right|\right)^2 \dfrac{p_{at}}{\kappa_s} \end{cases} \tag{A5}$$

From the 2nd equation in Eq.(A5), the modified swelling index κ_s corresponding to any average equivalent strain level can be obtained as

$$\kappa_s = \frac{3(1-2\upsilon)(1+e_0)}{2(1+\upsilon)}\left(1+P_{\text{rev}}\frac{3}{7}\left|\frac{\varepsilon_{eq}^{*}}{\varepsilon_{70}}\right|\right)^2\frac{p_{at}}{G_{ref\,0}} \tag{A6}$$

This equation suggests that the apparent swelling index increases (corresponding to the decrease of shear modulus and bulk modulus) with the increasing of average equivalent strain.

References

1. Juang C, Hsein , Luo Z, Atamturktur S, Huang H (2012) Bayesian updating of soil parameters for braced excavations using field observations. Journal of geotechnical and geoenvironmental engineering 139 (3):395-406
2. Ou C-Y, Liao J-T, Lin H-D (1998) Performance of diaphragm wall constructed using top-down method. Journal of geotechnical and geoenvironmental engineering 124 (9):798-808
3. Shen S, Wang Z, Cheng W (2017) Estimation of lateral displacement induced by jet grouting in clayey soils. Géotechnique 67 (7):621-630
4. Shen S-L, Xu Y-S (2011) Numerical evaluation of land subsidence induced by groundwater pumping in Shanghai. Canadian Geotechnical Journal 48 (9):1378-1392
5. Kung TC, Hsiao CL, Junag CH (2007) Evaluation of a simplified small-strain soil model for analysis of excavation-induced movements. Canadian Geotechnical Journal 44 (6):726-736
6. Kung TC, Ou CY, Juang CH (2009) Modeling small-strain behavior of Taipei clays for finite element analysis of braced excavations. Computers & Geotechnics 36 (1-2):304-319
7. Teng FC, Ou CY, Hsieh PG (2014) Measurements and Numerical Simulations of Inherent Stiffness Anisotropy in Soft Taipei Clay. Journal of Geotechnical & Geoenvironmental Engineering 140 (1):237-250
8. Shen S-L, Wu H-N, Cui Y-J, Yin Z-Y (2014) Long-term settlement behaviour of metro tunnels in the soft deposits of Shanghai. Tunnelling and Underground Space Technology 40:309-323
9. Xu Y-S, Shen S-L, Ren D-J, Wu H-N (2016) Analysis of factors in land subsidence in Shanghai: a view based on a strategic environmental assessment. Sustainability 8 (6):573
10. Jin Y-F, Yin Z-Y, Shen S-L, Hicher P-Y (2016) Selection of sand models and identification of parameters using an enhanced genetic algorithm. Int J Numer Anal Methods Geomech 40 (8):1219-1240. doi:10.1002/nag.2487
11. de Bragança Pereira CA, Stern JM (2001) Model selection: full Bayesian approach. Environmetrics 12 (6):559-568
12. Beck JL, Yuen K-V (2004) Model selection using response measurements: Bayesian probabilistic approach. Journal of engineering mechanics 130 (2):192-203
13. Cao Z, Wang Y (2014) Bayesian model comparison and selection of spatial correlation functions for soil parameters. Structural Safety 49:10-17
14. Zhang J, Zhang LM, Tang WH (2009) Bayesian Framework for Characterizing Geotechnical Model Uncertainty. Journal of Geotechnical and Geoenvironmental Engineering 135 (7):932-940. doi:doi:10.1061/(ASCE)GT.1943-5606.0000018
15. Zhang R, Mahadevan S (2000) Model uncertainty and Bayesian updating in reliability-based inspection. Structural Safety 22 (2):145-160
16. Tan F, Zhou W-H, Yuen K-V (2016) Modeling the soil water retention properties of same-textured soils with different initial void ratios. J Hydrol 542:731-743
17. Yuen K-V (2010) Recent developments of Bayesian model class selection and applications in civil engineering. Structural Safety 32 (5):338-346

18. Jin Y-F, Wu Z-X, Yin Z-Y, Shen JS (2017) Estimation of critical state-related formula in advanced constitutive modeling of granular material. Acta Geotech doi:10.1007/s11440-017-0586-5
19. Jin Y-F, Yin Z-Y, Riou Y, Hicher P-Y (2017) Identifying creep and destructuration related soil parameters by optimization methods. KSCE Journal of Civil Engineering 21 (4):1123-1134. doi:10.1007/s12205-016-0378-8
20. Jin Y-F, Yin Z-Y, Shen S-L, Hicher P-Y (2016) Investigation into MOGA for identifying parameters of a critical-state-based sand model and parameters correlation by factor analysis. Acta Geotech 11 (5):1131-1145. doi:10.1007/s11440-015-0425-5
21. Jin Y-F, Yin Z-Y, Shen S-L, Zhang D-M (2017) A new hybrid real-coded genetic algorithm and its application to parameters identification of soils. Inverse Problems in Science and Engineering 25 (9):1343-1366. doi:10.1080/17415977.2016.1259315
22. Yin Z-Y, Jin Y-F, Shen JS, Hicher P-Y (2017) Optimization techniques for identifying soil parameters in geotechnical engineering: Comparative study and enhancement. Int J Numer Anal Methods Geomech n/a-n/a. doi:10.1002/nag.2714
23. Yin Z-Y, Jin Y-F, Shen S-L, Huang H-W (2016) An efficient optimization method for identifying parameters of soft structured clay by an enhanced genetic algorithm and elastic–viscoplastic model. Acta Geotech 1-19. doi:10.1007/s11440-016-0486-0
24. Hsiao EC, Schuster M, Juang CH, Kung GT (2008) Reliability analysis and updating of excavation-induced ground settlement for building serviceability assessment. Journal of Geotechnical and Geoenvironmental Engineering 134 (10):1448-1458
25. Qi X-H, Zhou W-H (2017) An efficient probabilistic back-analysis method for braced excavations using wall deflection data at multiple points. Computers and Geotechnics 85:186-198
26. Finno RJ, Calvello M (2005) Supported excavations: observational method and inverse modeling. Journal of geotechnical and geoenvironmental engineering 131 (7):826-836
27. Zhao B, Zhang L, Jeng D, Wang J, Chen J (2015) Inverse analysis of deep excavation using differential evolution algorithm. Int J Numer Anal Methods Geomech 39 (2):115-134
28. Huang Z, Zhang L, Cheng S, Zhang J, Xia X (2014) Back-Analysis and Parameter Identification for Deep Excavation Based on Pareto Multiobjective Optimization. Journal of Aerospace Engineering 28 (6):A4014007
29. Jin Y-F, Yin Z-Y, Zhou W-H, Huang H-W (2019) Multi-objective optimization-based updating of predictions during excavation. Eng Appl Artif Intell 78:102-123. doi:https://doi.org/10.1016/j.engappai.2018.11.002
30. Levasseur S, Malécot Y, Boulon M, Flavigny E (2008) Soil parameter identification using a genetic algorithm. Int J Numer Anal Methods Geomech 32 (2):189-213. doi:10.1002/nag.614
31. Roscoe KH, Burland J (1968) On the generalized stress-strain behaviour of wet clay. Paper presented at the Engineering Plasticity, Cambridge, UK,
32. Sheng D, Sloan S, Yu H (2000) Aspects of finite element implementation of critical state models. Comput Mech 26 (2):185-196
33. Yao Y, Hou W, Zhou A (2009) UH model: three-dimensional unified hardening model for overconsolidated clays. Geotechnique 59 (5):451-469

34. Yao Y, Lu D, Zhou A, Zou B (2004) Generalized non-linear strength theory and transformed stress space. Sci China Ser E: Technol Sci 47 (6):691-709
35. Yao Y, Sun D, Matsuoka H (2008) A unified constitutive model for both clay and sand with hardening parameter independent on stress path. Computers and Geotechnics 35 (2):210-222
36. Franzius J, Potts D, Burland J (2005) The influence of soil anisotropy and K 0 on ground surface movements resulting from tunnel excavation. Géotechnique 55 (3):189-199
37. Hou Y, Wang J, Zhang L (2009) Finite-element modeling of a complex deep excavation in Shanghai. Acta Geotech 4 (1):7-16
38. Wheeler SJ, Näätänen A, Karstunen M, Lojander M (2003) An anisotropic elastoplastic model for soft clays. Canadian Geotechnical Journal 40 (2):403-418
39. Leoni M, Karstunen M, Vermeer P, MRTN-CT E (2009) Anisotropic creep model for soft soils. Geotechnique 58 (3):215-266
40. Yin ZY, Chang CS, Karstunen M, Hicher PY (2010) An anisotropic elastic-viscoplastic model for soft clays. Int J Solids Struct 47 (5):665-677
41. Yin ZY, Karstunen M, Chang CS, Koskinen M, Lojander M (2011) Modeling Time-Dependent Behavior of Soft Sensitive Clay. Journal of geotechnical and geoenvironmental engineering 137 (11):1103-1113. doi:10.1061/(asce)gt.1943-5606.0000527
42. Graham J, Houlsby G (1983) Anisotropic elasticity of a natural clay. Geotechnique 33 (2):165-180
43. Hoque E, Tatsuoka F (1998) Anisotropy in elastic deformation of granular materials. Soils and Foundations 38 (1):163-179
44. Hicher P-Y, Chang CS (2005) Evaluation of two homogenization techniques for modeling the elastic behavior of granular materials. Journal of engineering mechanics 131 (11):1184-1194
45. Schädlich B, Schweiger HF (2012) Influence of anisotropic small strain stiffness on the deformation behavior of geotechnical structures. Int J Geomech 13 (6):861-868
46. Benz T (2007) Small-strain stiffness of soils and its numerical consequences, vol 5. Univ. Stuttgart, Inst. f. Geotechnik,
47. Allman M, Atkinson J (1992) Mechanical properties of reconstituted Bothkennar soil. Géotechnique 42 (2):289-301
48. Hattab M, Hicher P-Y (2004) Dilating behaviour of overconsolidated clay. Soils and Foundations 44 (4):27-40
49. Hardin BO, Drnevich VP (1972) Shear modulus and damping in soils: Measurement and parameter effects (Terzaghi Leture). Journal of the Soil Mechanics and Foundations Division 98 (6):603-624
50. Yin Z-Y, Xu Q, Hicher P-Y (2013) A simple critical-state-based double-yield-surface model for clay behavior under complex loading. Acta Geotech 8 (5):509-523
51. Calvello M, Finno RJ (2004) Selecting parameters to optimize in model calibration by inverse analysis. Computers and Geotechnics 31 (5):410-424. doi:10.1016/j.compgeo.2004.03.004
52. Poles S, Fu Y, Rigoni E (2009) The effect of initial population sampling on the convergence of multi-objective genetic algorithms. In: Multiobjective Programming and Goal Programming. Springer, Berlin Heidelberg, pp 123-133

53. Sobol IM (1967) On the distribution of points in a cube and the approximate evaluation of integrals. USSR Computational Mathematics and Mathematical Physics 7 (4):86-112
54. Holland J (1992) Adaptation in natural and artificial systems. MIT Press, Cambridge, MA,
55. Ou C-Y, Shiau B-Y, Wang I-W (2000) Three-dimensional deformation behavior of the Taipei National Enterprise Center (TNEC) excavation case history. Canadian Geotechnical Journal 37 (2):438-448
56. Lim A, Ou CY, Hsieh PG (2010) Evaluation of clay constitutive models for analysis of deep excavation under undrained conditions. Journal of Geoengineering 5
57. Zhang L, Zuo Z, Ye G, Jeng D, Wang J (2013) Probabilistic parameter estimation and predictive uncertainty based on field measurements for unsaturated soil slope. Computers and Geotechnics 48:72-81
58. Tan F, Zhou WH, Yuen KV (2018) Effect of loading duration on uncertainty in creep analysis of clay. Int J Numer Anal Methods Geomech 42 (11):1235-1254
59. Zhou W-H, Tan F, Yuen K-V (2018) Model updating and uncertainty analysis for creep behavior of soft soil. Computers and Geotechnics 100:135-143. doi:https://doi.org/10.1016/j.compgeo.2018.04.006
60. Vucetic M, Dobry R (1991) Effect of soil plasticity on cyclic response. Journal of geotechnical engineering 117 (1):89-107
61. Yin Z-Y, Gu X-Q, Jin Y-F (2017) Small strain stiffness of soils. Tongji University press, Shanghai

Tables

Table 1 Summary of soil models for simulating clay behaviors

Model name	MCC	Anisotropic plasticity	Anisotropic elasticity	Small strain stiffness	Model abbreviation	Parameters to be optimized
Model-1	YES	-	-	-	MCC	υ
Model-2	YES	YES	-	-	S-CLAY1	υ
Model-3	YES	-	YES	-	MCC-AE	υ, n
Model-4	YES	-	-	YES	MCC-SS	υ, ε_{70}
Model-5	YES	YES	YES	-	S-CLAY1-AE	υ, n
Model-6	YES	YES	-	YES	S-CLAY1-SS	υ, ε_{70}
Model-7	YES	YES	YES	YES	S-CLAY1-AE-SS	υ, n, and ε_{70}

Table 2 Parameters of MC used in the finite element analysis

Depth (m)	γ (kN/m3)	c (kPa)	ϕ'(°)	ψ(°)	E (MPa)	K_0	υ
5.6–8.0	18.9	0	30	0	6.8	0.49	0.3
33.0–35.0	19.6	0	33	0	26.5	0.49	0.3
37.5–46.0	19.6	0	35	0	30.0	0.47	0.3

Table 3 Parameters of adopted soil model used in the finite element analysis

Depth (m)	γ (kN/m3)	λ	κ	e_0	M	K_0	υ	ε_{70}	n
0–5.6	18.3	0.10	0.012	1.067	1.09	1.0	[0.1, 0.4]	[10^{-6}, 10^{-3}]	[0.1, 3.0]
8.0–33.0	18.9	0.15	0.018	0.820	1.02	0.70	[0.1, 0.4]	[10^{-6}, 10^{-3}]	[0.1, 3.0]
35.0–37.5	18.2	0.10	0.012	0.824	1.05	0.52			

Figure captions

Figure 1

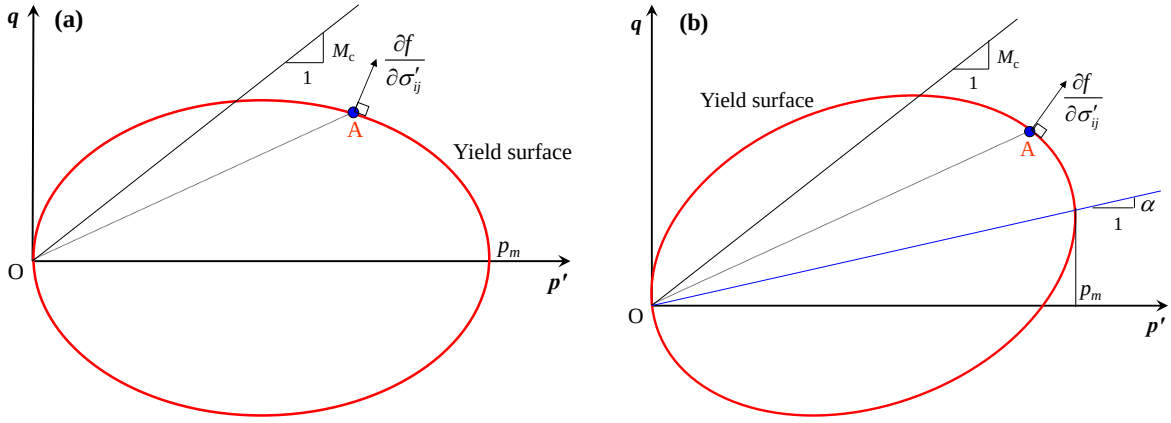
q
(a)
M_c
1
$\frac{\partial f}{\partial \sigma'_{ij}}$
A
Yield surface
O
p_m
p′
q
(b)
Yield surface
M_c
1
$\frac{\partial f}{\partial \sigma'_{ij}}$
A
α
1
O
p_m
p′

Figure 2

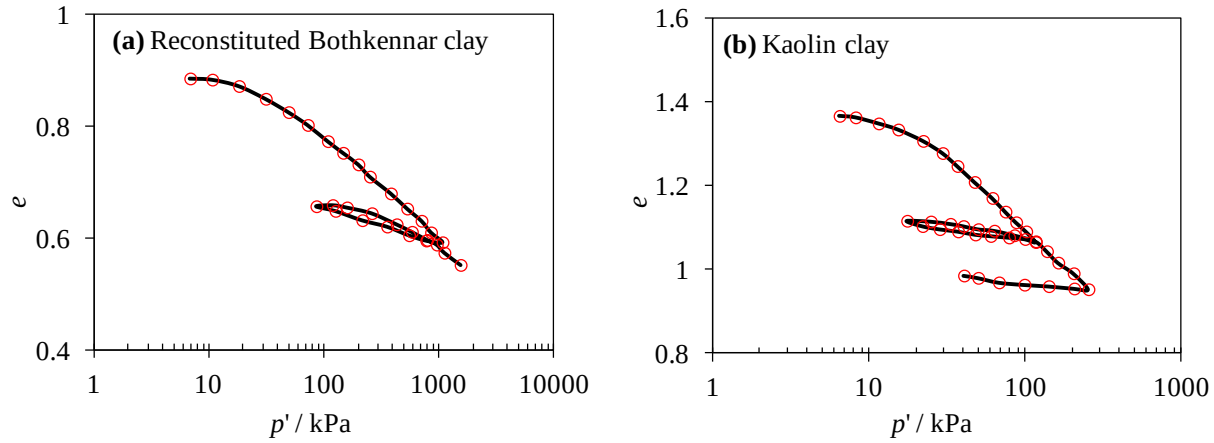
(a) Reconstituted Bothkennar clay
e
p' / kPa
1
0.8
0.6
0.4
1
10
100
1000
10000
(b) Kaolin clay
e
p' / kPa
1.6
1.4
1.2
1
0.8
1
10
100
1000

Figure 3

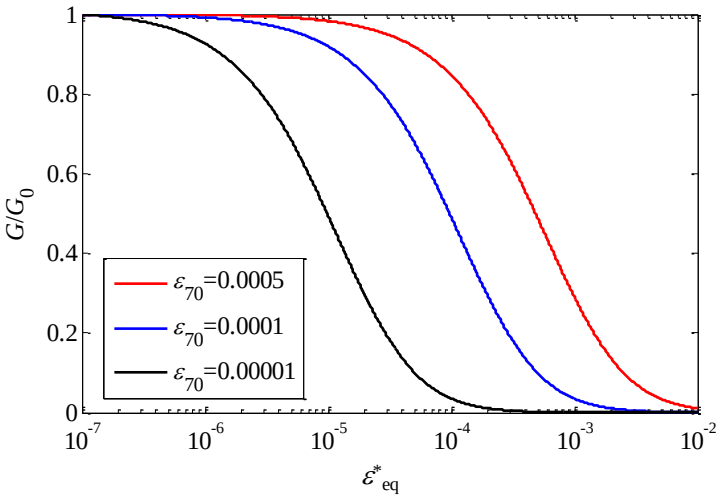
1
0.8
0.6
0.4
0.2
0
G/G_0
ε_{70}=0.0005
ε_{70}=0.0001
ε_{70}=0.00001
10^{-7}
10^{-6}
10^{-5}
10^{-4}
10^{-3}
10^{-2}
ε^*_{eq}

Figure 4

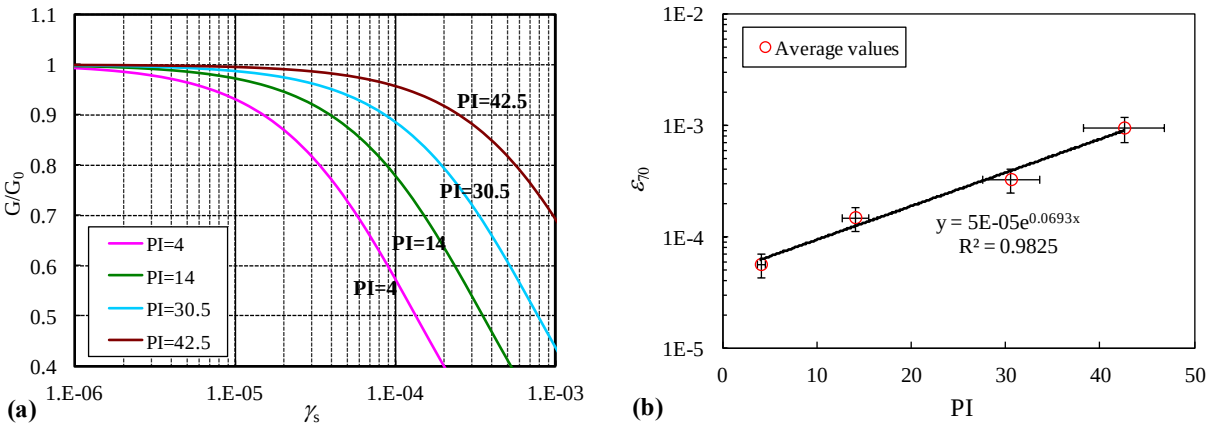
1.1
1
0.9
0.8
0.7
0.6
0.5
0.4
G/G0
PI=4
PI=14
PI=30.5
PI=42.5
PI=42.5
PI=30.5
PI=14
PI=4
1.E-06
1.E-05
1.E-04
1.E-03
γs
(a)
1E-2
1E-3
1E-4
1E-5
ε70
Average values
y = 5E-05e0.0693x
R² = 0.9825
0
10
20
30
40
50
PI
(b)

Figure 5

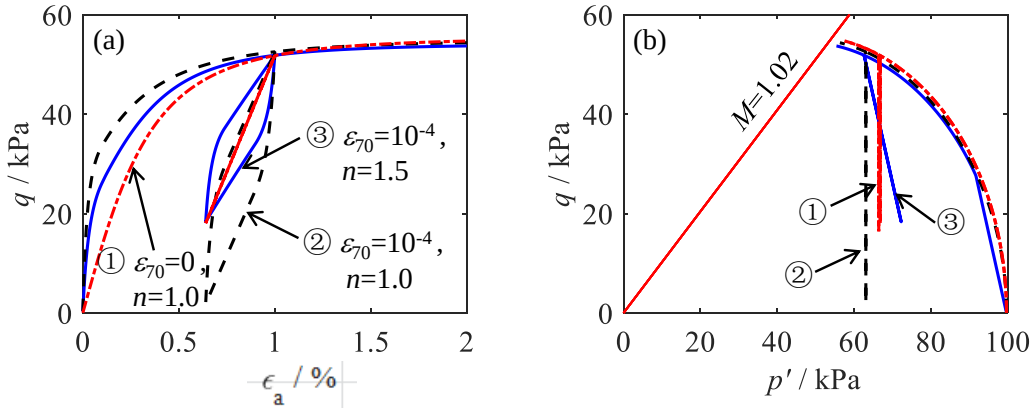
(a)
q / kPa
60
40
20
0
0
0.5
1
1.5
2
ϵa / %
① ε70=0, n=1.0
② ε70=10-4, n=1.0
③ ε70=10-4, n=1.5
(b)
M=1.02
p′ / kPa
0
20
40
60
80
100

Figure 6

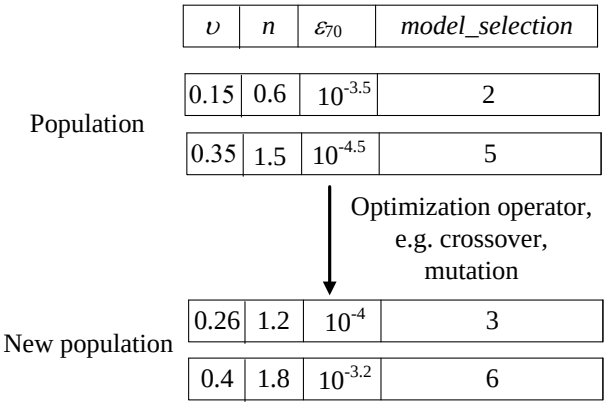
υ
n
ε70
model_selection
Population
0.15
0.6
10-3.5
2
0.35
1.5
10-4.5
5
Optimization operator, e.g. crossover, mutation
New population
0.26
1.2
10-4
3
0.4
1.8
10-3.2
6

Figure 7

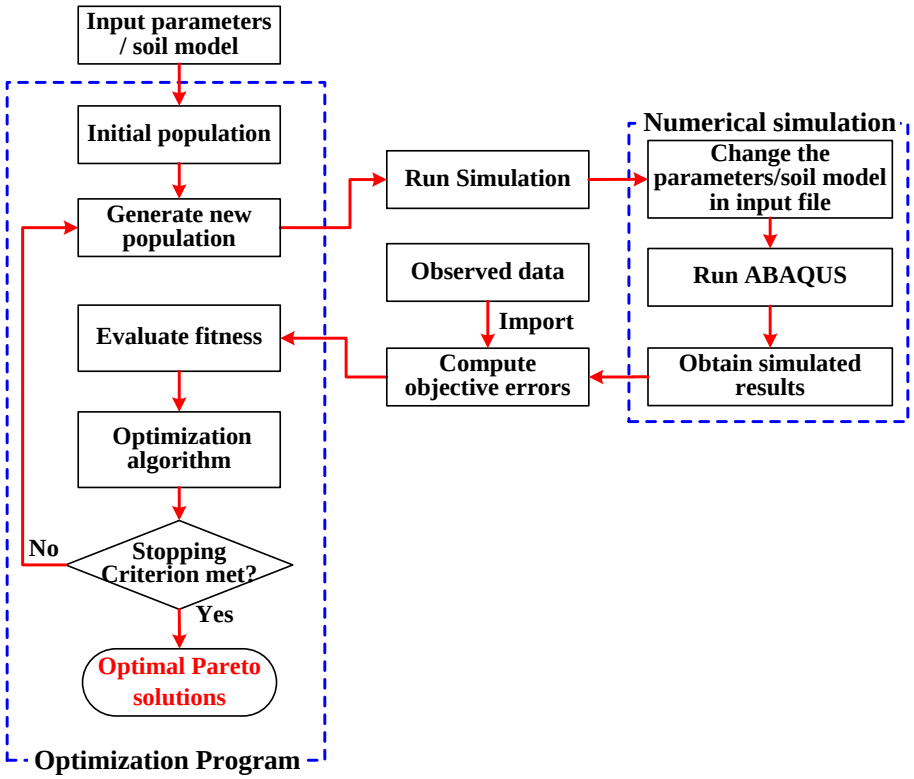
Input parameters / soil model
Initial population
Generate new population
Evaluate fitness
Optimization algorithm
Stopping Criterion met?
No
Yes
Optimal Pareto solutions
Optimization Program
Run Simulation
Observed data
Import
Compute objective errors
Numerical simulation
Change the parameters/soil model in input file
Run ABAQUS
Obtain simulated results

Figure 8

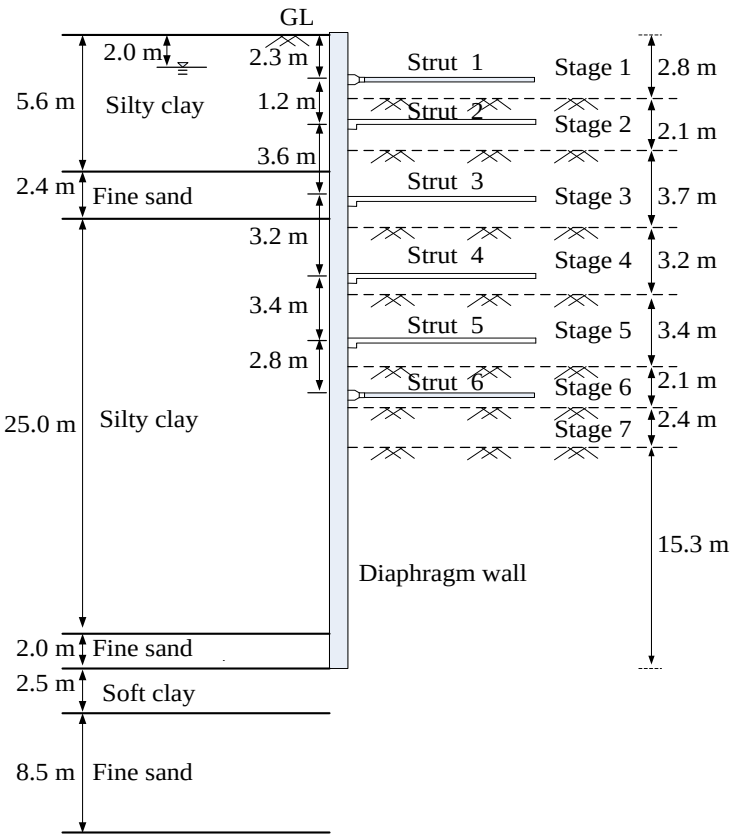
GL
2.0 m
2.3 m
Strut 1
Stage 1
2.8 m
5.6 m
Silty clay
1.2 m
Strut 2
Stage 2
2.1 m
3.6 m
2.4 m
Fine sand
Strut 3
Stage 3
3.7 m
3.2 m
Strut 4
Stage 4
3.2 m
3.4 m
Strut 5
Stage 5
3.4 m
2.8 m
Strut 6
Stage 6
2.1 m
25.0 m
Silty clay
Stage 7
2.4 m
15.3 m
Diaphragm wall
2.0 m
Fine sand
2.5 m
Soft clay
8.5 m
Fine sand

Figure 9

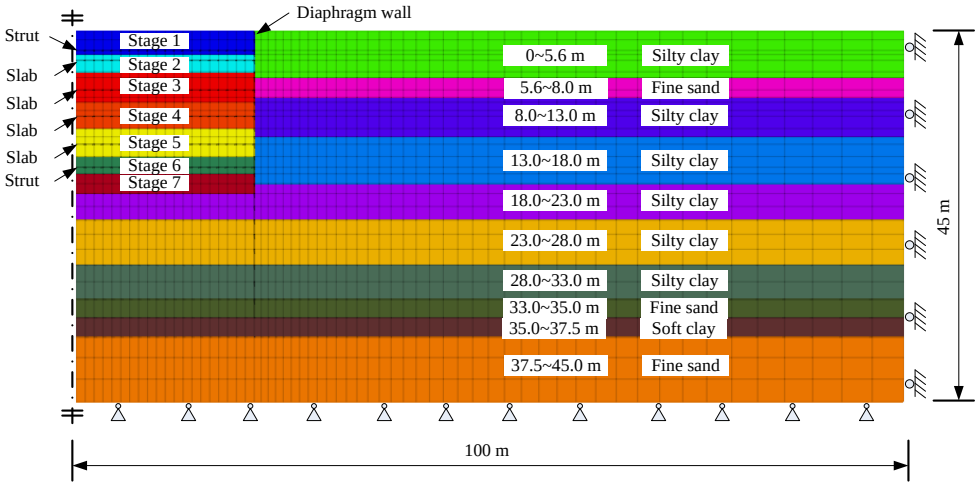
Diaphragm wall
Strut
Slab
Slab
Slab
Strut
Stage 1
Stage 2
Stage 3
Stage 4
Stage 5
Stage 6
Stage 7
0~5.6 m
Silty clay
5.6~8.0 m
Fine sand
8.0~13.0 m
Silty clay
13.0~18.0 m
Silty clay
18.0~23.0 m
Silty clay
23.0~28.0 m
Silty clay
28.0~33.0 m
Silty clay
33.0~35.0 m
Fine sand
35.0~37.5 m
Soft clay
37.5~45.0 m
Fine sand
45 m
100 m

Figure 10

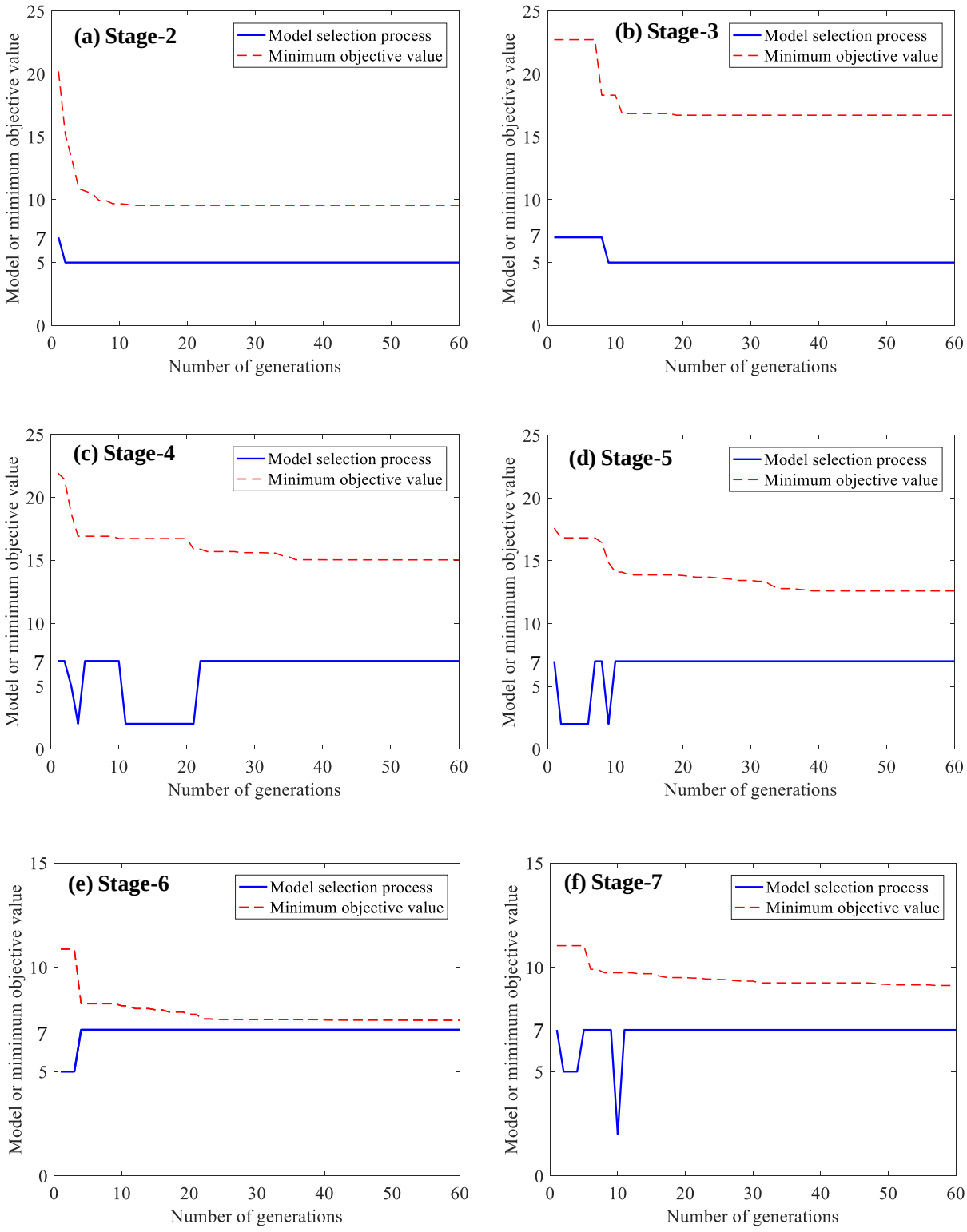
(a) Stage-2
(b) Stage-3
(c) Stage-4
(d) Stage-5
(e) Stage-6
(f) Stage-7
Model selection process
Minimum objective value
Model or mimimum objective value
Number of generations

Figure 11

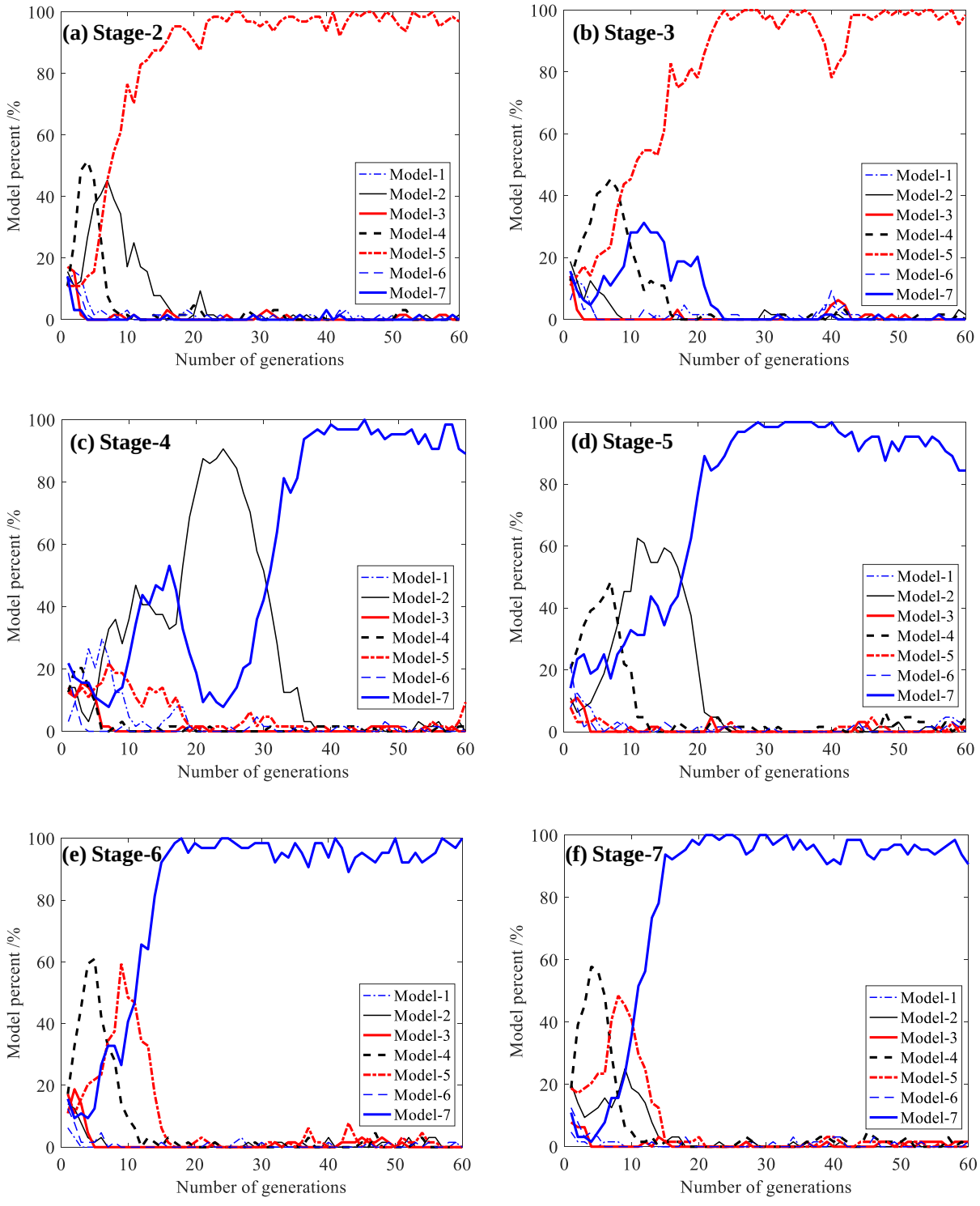
(a) Stage-2
(b) Stage-3
(c) Stage-4
(d) Stage-5
(e) Stage-6
(f) Stage-7
Model percent /%
Number of generations
Model-1
Model-2
Model-3
Model-4
Model-5
Model-6
Model-7

Figure 12

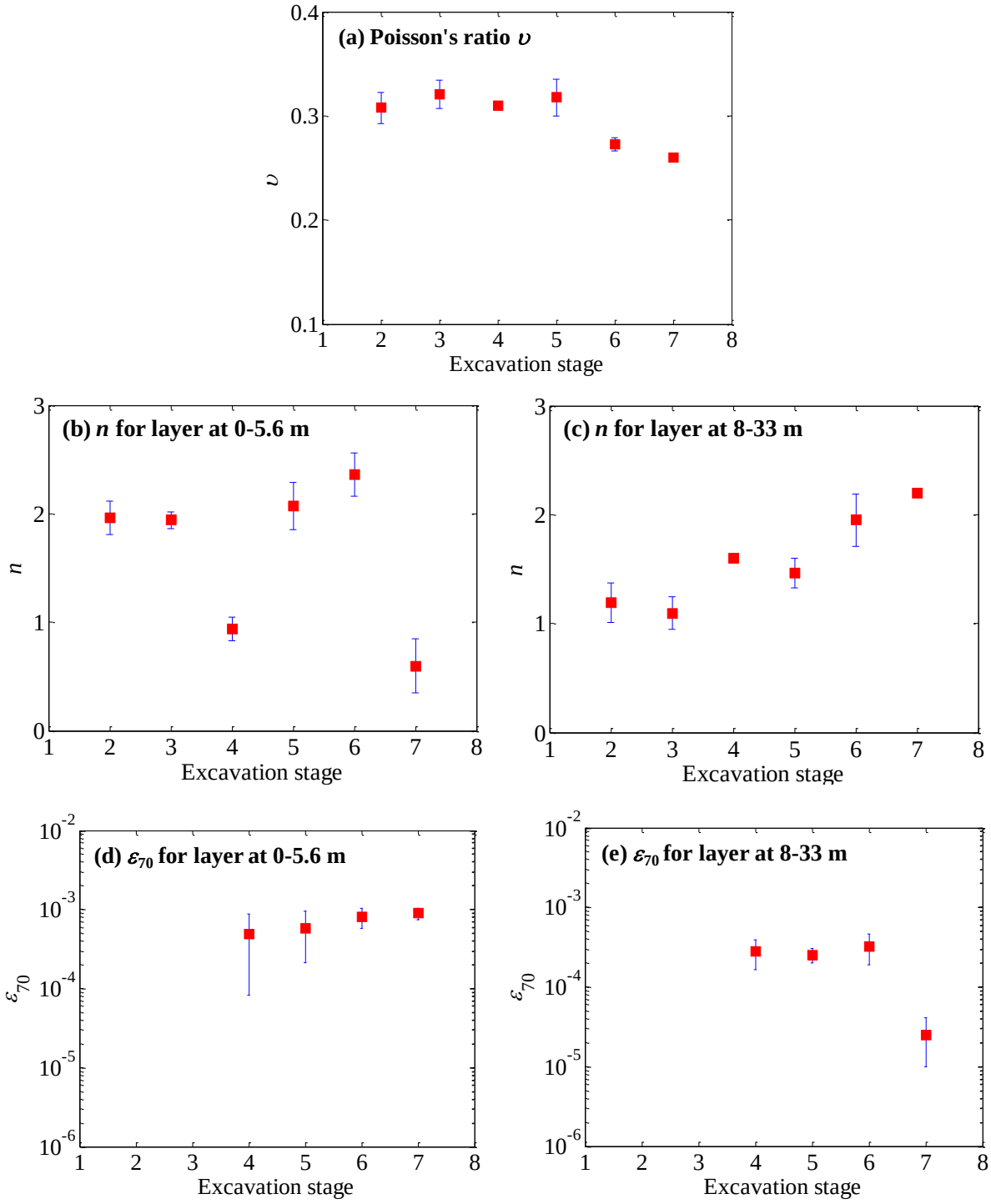
(a) Poisson's ratio υ
υ
Excavation stage
(b) n for layer at 0-5.6 m
n
Excavation stage
(c) n for layer at 8-33 m
n
Excavation stage
(d) ε70 for layer at 0-5.6 m
ε70
Excavation stage
(e) ε70 for layer at 8-33 m
ε70
Excavation stage

Figure 13

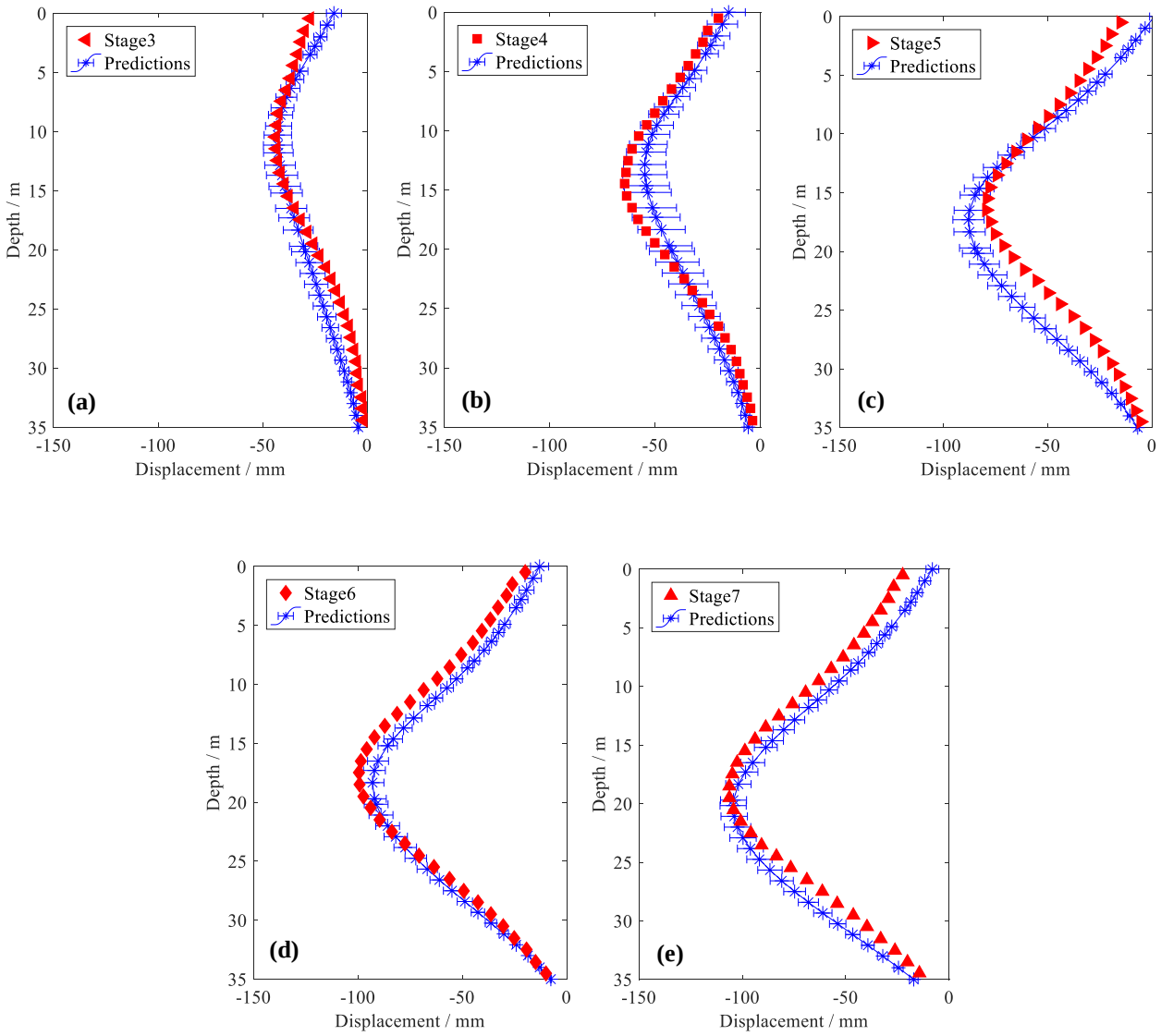
Stage3
Predictions
(a)
Stage4
Predictions
(b)
Stage5
Predictions
(c)
Stage6
Predictions
(d)
Stage7
Predictions
(e)
Depth / m
Displacement / mm
0
5
10
15
20
25
30
35
-150
-100
-50
0

Figure 14

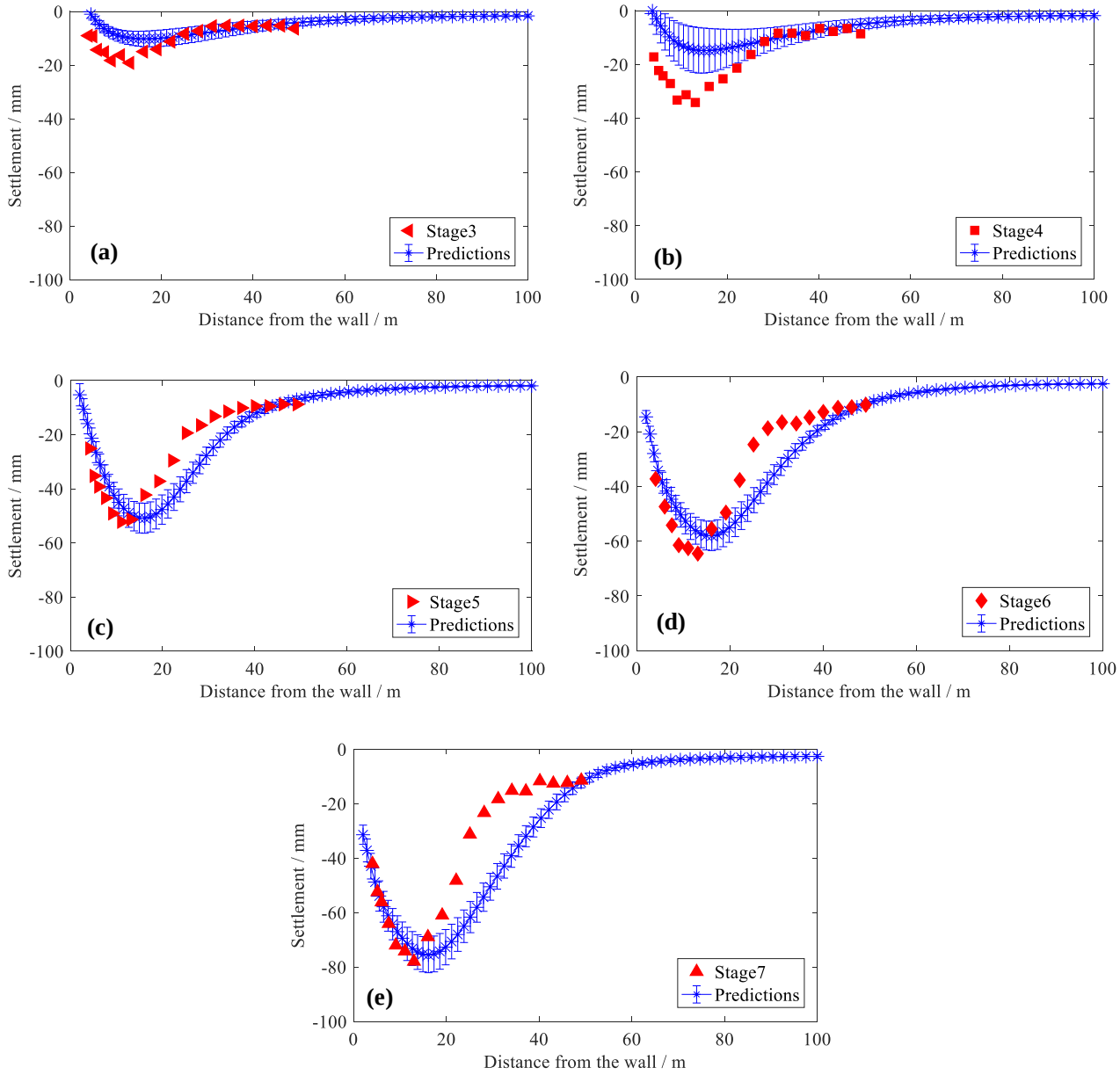
Settlement / mm
Distance from the wall / m
(a)
Stage3
Predictions
(b)
Stage4
Predictions
(c)
Stage5
Predictions
(d)
Stage6
Predictions
(e)
Stage7
Predictions